Asymmetric Dehydrative Cyclization of Allyl Alcohol to Cyclic Ether Using Chiral Brønsted Acid/CpRu(II) Hybrid Catalysts: DFT Study of the Origin of Enantioselectivity

Manussada Ratanasak,[1] *Shinji Tanaka,*[2] *Masato Kitamura,*,*[3] *Jun-ya Hasegawa*,*[1,2]

[1] Institute for Catalysis, Hokkaido University, Kita 21, Nishi 10, Kita-ku, Sapporo 001-0021, Japan

[2] Interdisciplinary Research Center for Catalytic Chemistry National Institute of Advanced Industrial Science and Technology, Central 5, 1-1-1 Higashi, Tsukuba, Ibaraki 305-8565, Japan

[3] Research Center for Materials Science, Nagoya University, Chikusa, Nagoya 464-8602, Japan

E-mail: manussada@cat.hokudai.ac.jp, tanaka-sh@aist.go.jp
kitamura@os.rcms.nagoya-u.ac.jp, hasegawa@cat.hokudai.ac.jp

Keywords

Enantioselectivity, Dehydrative allylation, Halogen dependency, Ruthenium, DFT calculations

Abstract

To elucidate the reaction mechanism and the origin of the enantioselectivity of the asymmetric dehydrative cyclization of allyl alcohol to cyclic ether catalyzed by a Cp-ruthenium complex and a chiral pyridinecarboxylic acid, (*R*)-X-Naph-PyCOOH, denisity functional theory (DFT) calculations were performed. According to the DFT calculations, the rate-determining step is the dehydrative σ-allyl formation with $\Delta G^{\ddagger}$ = 18.1 kcal mol^{-1} at 80 °C. This agrees well with the experimental data ($\Delta G^{\ddagger}$ = 19.01 kcal mol^{-1} at 80 °C). The DFT result showed that both hydrogen and halogen bonds play a key role in the high enantioselectivity by facilitating the major *R*,*S*$_{Ru}$-catalyzed reaction pathway via a σ-allyl Ru intermediate to generate the major (*S*)-product. In contrast, the reaction is sluggish in the presence of the diastereomeric *R*,*R*$_{Ru}$ catalyst with an apparent activation energy of 33.1 kcal mol^{-1}; the minor (*R*)-product is formed via a typical π-allyl Ru intermediate and via a minor pathway for the cyclization step. In addition, the calculated activation Gibbs free energies, 14.4 kcal mol^{-1} for I < 16.8 kcal mol^{-1} for Br < 18.1 kcal mol^{-1} for Cl, reproduced the observed halogen dependent reactivity with the (*R*)-X-Naph-PyCOOH ligands. The origin of the halogen trend was clarified by a structural decomposition analysis.

1. Introduction

Asymmetric Tsuji–Trost allylation reaction is one of the key catalytic reactions for the synthesis of chiral compounds.[1] Among the transition metal catalysts for asymmetric allylation reactions,[2-9] Palladium is the most commonly used transition metal for the activation of allylic alcohols toward nucleophilic attack.[10] Tsuji reported the first palladium-catalyzed allylic substitution reactions of allylic alcohols were reported in 1964.[11] Allylic alcohols are a substantially less expensive substrates and were found to be the most reactive species compared to their activated counterparts. Sundararaju et al.[12] have described the transition metal-catalyzed nucleophilic allylic substitution of allylic alcohols via π-allylic species in detail. Direct activation of allylic alcohols in the presence of transition metal catalysts produces electrophilic π-allyl metal intermediates.

Many studies[13-19] have been conducted to discover novel catalysts for asymmetric allylations. A major challenge has been elucidation of the reaction mechanism and the origin of the enantioselectivity of the allylation reactions for both experimental and theoretical chemists. So far, the reaction mechanism commonly involves π-allylic intermediate. For instance, Piechaczyk et al.[20] reported a DFT study of palladium-catalyzed allylation of primary amines. They reported two potential mechanisms. The first mechanism is based on the formation of a cationic Pd hydride species whereas the second mechanism is based on the decomplexation of the coordinated allylammonium ligand. The second mechanism was consistent with the results of the theoretical and experimental studies on the electronic influence of ligands. Zhang et al.[21] used DFT calculations to investigate the mechanism of allylic alkylation of simple ketones and allylic alcohols. According to their calculations, methanol is required for the C-O bond cleavage via hydrogen bond activation. Moreover, solvents were found to play an important role in the formation of the π-allylpalladium complex and could be reduced the energy barrier. McPherson et al.[22] used DFT calculations to investigate the mechanistic of an enantioselective Tsuji−Trost allylation reaction of allyl enol carbonate. As the key species in the plausible reaction pathways, they suggested a square-planar palladium allyl enolate intermediate. Additionally, their results revealed that water is crucial in the

preferential stabilization of a keto-coordinated adduct of the Pd(II)-η^1-allyl complex. In the last decade, ruthenium catalysts have been used more frequently than palladium catalysts for the direct substitution of allylic alcohols.[23-25] The Ru-catalyzed allylic alkylation reaction has attracted significant interest because of its regioselectivity for branched allylic products. The first reported ruthenium pre-catalyst, $[RuCl_2(PPh_3)_3]$, was used to form allylic ethers from homoallylic alcohols and glycols.[23] Mechanistic studies for the Ru catalyst also introduced π-allylic intermediate species. Hermatschweiler et al.,[24] for example, reported a combined experimental and DFT study for the explanation of regioselectivity for the Ru-catalyzed allylic alkylation reaction.

Kitamura group[25] recently reported an allylation reaction in which a key role of a σ-allyl Ru intermediate was pointed out for the first time in this class of reactions. For catalytic asymmetric reactions, a Ru(II)/Ru(IV) redox allylation system with chirality-modified picolinic acid (pyCOOH) ligands was used. They developed the (*R*)-Cl-Naph-PyCOOH ligand (Naph: naphthalene, Py: pyridine) for a Trost-type CpRu complex, which enabled the intramolecular dehydrative cyclization of ω-hydroxy allyl alcohols to give alkenyl cyclic ethers with high enantioselectivity.[26-27] The advantage of the direct Ru–Allyl formation using the protic nucleophiles (NuH) and allylic alcohols (AllOH) is that the by-product is only H_2O, thus making their process environmentally benign and very atom- and step-economical.

As shown in Figure 1, the chiral Brønsted acid/CpRu(II) combined catalyst **1** exists as an equilibrium mixture of two diastereomers, (R,R_{Ru})-**1** (A_R) and (R,S_{Ru})-**1** (A_S), which originate due to the ligand chirality and the Ru stereogenic center.

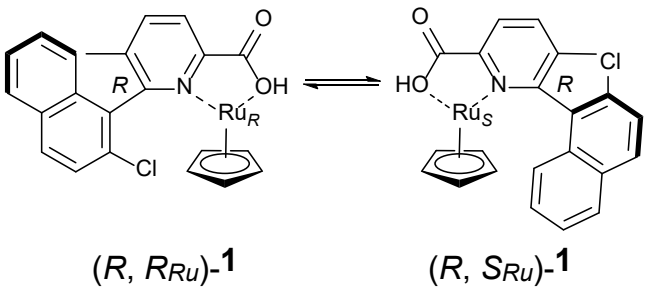

Figure 1. Chiral Brønsted acid/CpRu(II) combined catalyst (**1**) with (*R*)-Cl-Naph-PyCOOH ligand. Two diastereomers, (*R,R*$_{Ru}$)-**1** (A$_R$, left) and (*R,S*$_{Ru}$)-**1** (A$_S$, right), were identified.

In the previous report,[25] an experimental study was conducted for clarifying mechanism of conversion from (*E*)-hept-2-ene-1,7-diol (**2**) to (*S*)-2-vinyltetrahydro-2*H*-pyran ((*S*)-**3**) and (*R*)-2-vinyltetrahydro-2*H*-pyran ((*R*)-**3**) in an *S*/*R* enantiomeric ratio (er) of 97:3 er, as shown in Figure 2. NMR measurements suggested that the reaction proceeded via σ-allyl mechanism as a major pathway and π-allyl mechanism as a minor pathway. This is the first report of the σ-allyl pathway for the Ru-catalyzed allylation reactions.[25] However, no theoretical evidence was so far obtained.

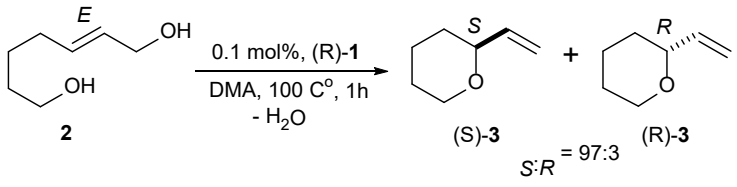

Figure 2. Conversion of (*E*)-hept-2-ene-1,7-diol (**2**) to (*S*)-2-vinyltetrahydro-2*H*-pyran ((*S*)-**3**) and (*R*)-2-vinyltetrahydro-2*H*-pyran ((*R*)-**3**) products.

Based on our previous experimental results,[25] we performed DFT calculations to clarify the mechanistic details and elucidated the origin of the enantioselectivity of the asymmetric dehydrative cyclization of

allylic alcohol to cyclic ether catalyzed by a CpRu/Brønsted acid combined with chiral (*R*)-Cl-Naph-PyCOOH ligand. Moreover, we examined the halogen effect in the rate determining step (RDS) of the major σ-allyl mechanism on the reactivity. This paper shows a theoretical insight into the catalytic mechanism of the asymmetric dehydrative allylation involving an σ-allyl Ru intermediate which provides a substantially lower energy reaction pathway than π-allyl intermediate. The results of this study are consistent with our earlier experimental data[25] and can explain the origin of the strong enantioselectivity with chiral Brønsted acid/CpRu(II) hybrid catalysts.

2. Presently Proposed Mechanism and Notations

Here, our notations used in this paper are explained. In Scheme 1, the catalyst/substrate complex "B_S-*saSi*" denotes that C(3) substituent is syn to C(2)H and anti to the Ru carboxylato moiety, and the *Si* face of C(3) is directed to the Ru side; therefore, this is abbreviated as "syn,anti,*Si*" or "sa*Si*" hereafter. In the catalyst/substrate complex "B_S-*ssSi*", the C(3) substituent is syn to C(2)H and syn to the Ru carboxylato moiety and the *Si* face of C(3) is directed to the Ru side; therefore, this is abbreviated as "syn,syn,*Si*" or "ss*Si*" hereafter. Two modes of hydration have been revealed: H_2O liberation to the Ru side or "inside" (H_2O_{in}) and H_2O liberation from the Ru side or "outside" (H_2O_{out}). Moreover, there are two modes of the nucleophilic attacks in the intramolecular reductive nucleophilic attack of C(7)OH on the allyl C(3) carbon: "inside" attack (OH_{in}) and "outside" attack (OH_{out}).

As shown in Scheme 1, there are "$A_{S,in,in}$" and "$A_{R,out,out}$" cycles. The former means that the reaction cycle produces (*S*)-product via H_2O_{in} and OH_{in} processes, while the later means that (*R*)-product is formed via H_2O_{out} and OH_{out} processes. In the $A_{S,in,in}$ cycle (red), the major (*S*)-**3** product is generated from a σ-allyl intermediate involving a halogen bond. In the reactant state, A_S captures substrate **2** using two weak interactions hydrogen and halogen bonding to stabilize the catalyst/substrate complex S_{Ru}-R (B_S-*saSi*). The Ru catalyst performs as a redox-involved donor–acceptor bifunctional catalyst and facilitates the dehydrative σ-allyl formation of the intramolecularly activated **2** to Ru(II) via TS1 in an H_2O_{in} manner (S_{Ru}-

TS1-H_2O_{in}), resulting in the formation of the σ-allyl intermediate S_{Ru}-I1 (σ-C_S-sa*Si*). The two attractive interactions, hydrogen and halogen bonds, are kept and promote the formation of the σ-allyl complex. Then, the σ-allyl intermediate S_{Ru}-I1 changes conformation to the more stable σ-allyl intermediate S_{Ru}-I2 via the C-C bond rotation (S_{Ru}-TS2). The S_{Ru}-I2-OH_{in} state enables the nucleophilic OH_{in} "inside" attack to generate the major (*S*)-product through S_{Ru}-TS3-OH_{in}. Another possible pathway is shown in the pink path. The OH nucleophile can attack the C_3 of the allyl alcohol substrate from outside (S_{Ru}-I2-OH_{out}) via TS3 (S_{Ru}-TS3-OH_{out}) to generate a minor (*R*)-product complex.

In the $A_{R,out,out}$ cycle (black), the minor (*R*)-**3** product is generated via a conventional π-allyl mechanism. In contrast to A_S, the generation of R_{Ru}-R (B_R-*ssSi*) from A_R is energetically unfavorable due to both the lack of the σ-hole assistance by the Cl-O bond and the hydrogen bond. As a result, the A_R cycle slowly forms a conventional π-allyl intermediate R_{Ru}-I1 (C_R-*ssSi*) through the H_2O_{out} mechanism via TS1 (R_{Ru}-TS1-H_2O_{out}), followed by nucleophilic attack of the OH group through the OH_{out} mechanism via TS2 (R_{Ru}-TS2-OH_{out}), to yield the minor (*R*)-**3** product. The blue path represents another possible route. The OH nucleophile can attack the C_3 of the allyl alcohol substrate from the inside (R_{Ru}-I2-OH_{in}) via TS2 (R_{Ru}-TS2-OH_{in}), to generate a major (*S*)-product complex.

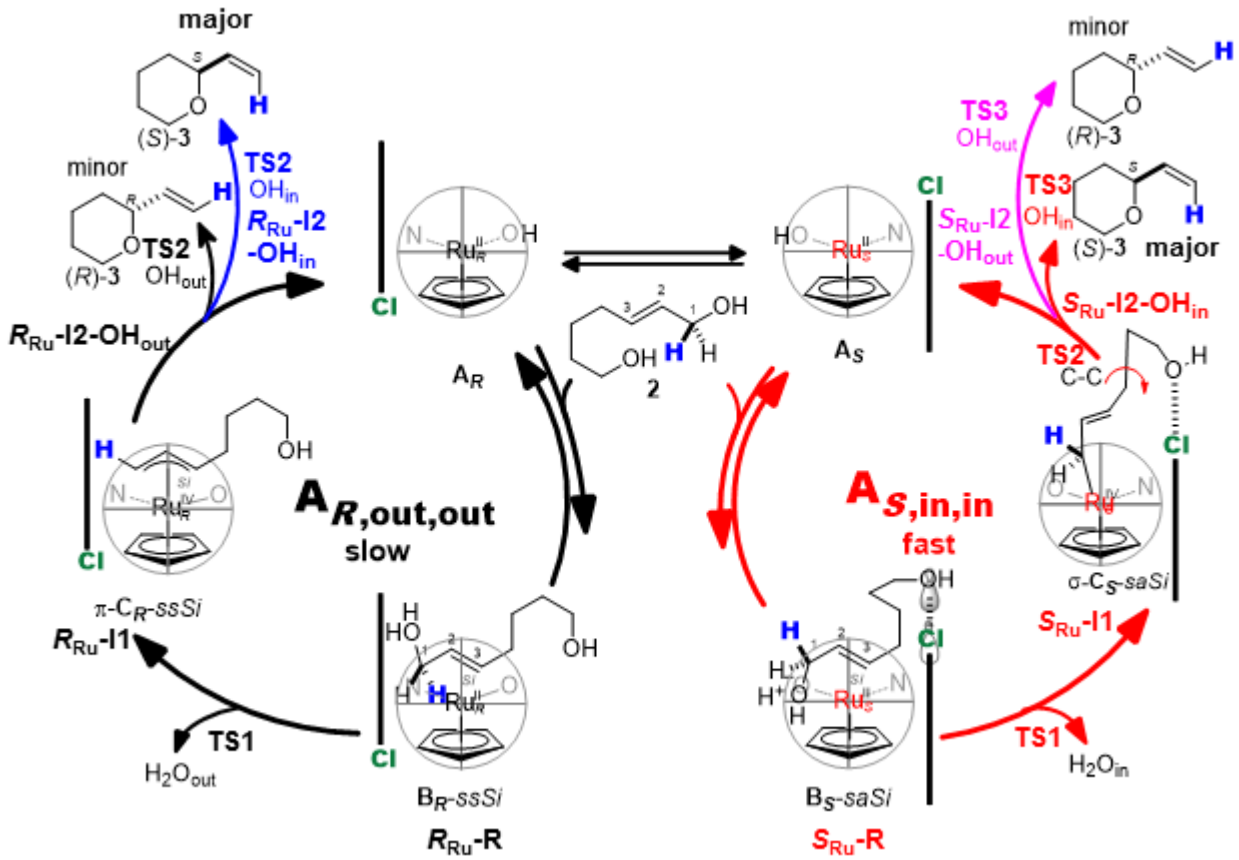

Scheme 1. A proposed mechanism for the CpRu-catalyzed asymmetric dehydrative intramolecular O-allylation of allyl alcohol **2** to cyclic ether **3** using (*R*)-Cl-Naph-PyCOOH ligand via major σ-allyl pathway (red), minor π-allyl mechanism (black) and possible routes OH_{out}, *R*-product (pink) with OH_{in}, *S*-product (blue).

3. Computational Details

All the DFT calculations were performed using the Gaussian 09 (Rev. E.01) program.[28] For the optimization of all structures, a range-separated hybrid functional with damped atom-atom dispersion (ωB97XD)[29] functionals with the 6-31G(d,p) basis set, and the effective core potential SDD[30] basis set for Ru and I atoms were employed. In order to obtain accurate potential energies, the single-point calculations were computed at the ωB97XD/6-311+G(2d,p), SDD for Ru and I atoms. Effect of the basis sets extension was given in Table S5 of the supporting information. The solvation effect of *N,N*-dimethylacetamide

(DMA) was evaluated by single-point calculations using the PCM model (ε = 37.7810 for DMA). To check whether an optimized structure is an energy minimum or a transition state, vibrational frequency calculations were performed on the optimized structures at the same level of theory. The Gibbs free energies were calculated at 298.15 K and 1 atmospheric pressure. The free energy barrier was calculated at the RDS and at 353K (80 °C) for comparison with experimental result. Chemcraft version 1.8 program was used to generate all the 3D images of the optimized structures.[31]

4. Results and Discussion

4.1. Relative Stability of A_R and A_S

Initially, the relative stabilities of the two diastereomers of the chiral Brønsted acid/CpRu(II) combined catalyst **1** were compared. A penta-coordinated Ru complex with the (*R*)-Cl-Naph-PyCOOH ligand coordinated at the OH group[25] is the computational model for **1**. Figure 3 depicts the optimized structures of R,R_{Ru} (A_R, left) and R,S_{Ru} (A_S, right). The followings are the definitions of potential energy, ΔE, and Gibbs energy, ΔG, relative to the optimized structures of R,R_{Ru}.

$$\Delta E = E(S_{Ru}) - E(R_{Ru})$$

$$\Delta G = G(S_{Ru}) - G(R_{Ru})$$

A positive / negative ΔE and ΔG value means that R_{Ru} / S_{Ru} is stable in energy.

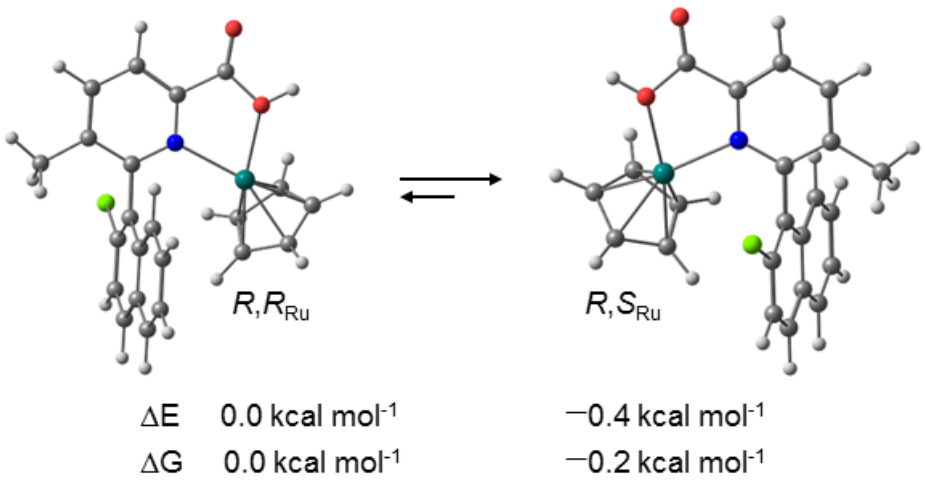

Figure 3. Optimized structures of the two diastereomers: R,R_{Ru} (A_R, left) and R,S_{Ru} (A_S, right). Potential energy and Gibbs energy relative to R,R_{Ru}.

Figure 3 shows that both ΔE (−0.4 kcal mol^{-1}) and ΔG (−0.2 kcal mol^{-1}) are negative, suggesting that S_{Ru} and R_{Ru} populate with a Boltzmann ratio of 56.4 : 43.6 at 353K based on the ΔG values. This result is qualitatively consistent with our experimental results showing that monocationic *R*, R_{Ru}, and *R*, S_{Ru} are swiftly converted to one other with K ≈ 1.[25]

4.2. Major σ-allyl and Minor π-allyl Mechanisms

In this section, we discuss major σ-allyl mechanism (pathway shown in red) and minor π-allyl mechanism (pathway shown in black) for the CpRu-catalyzed asymmetric dehydrative intramolecular O-allylation of alcohol to cyclic ether using the (*R*)-Cl-Naph-PyCOOH ligand (Scheme 1). The detailed potential energy profiles for the (*R*)-Cl-Naph-PyCOOH–CpRu-catalyzed intramolecular O-allylation are shown in Figure 4.

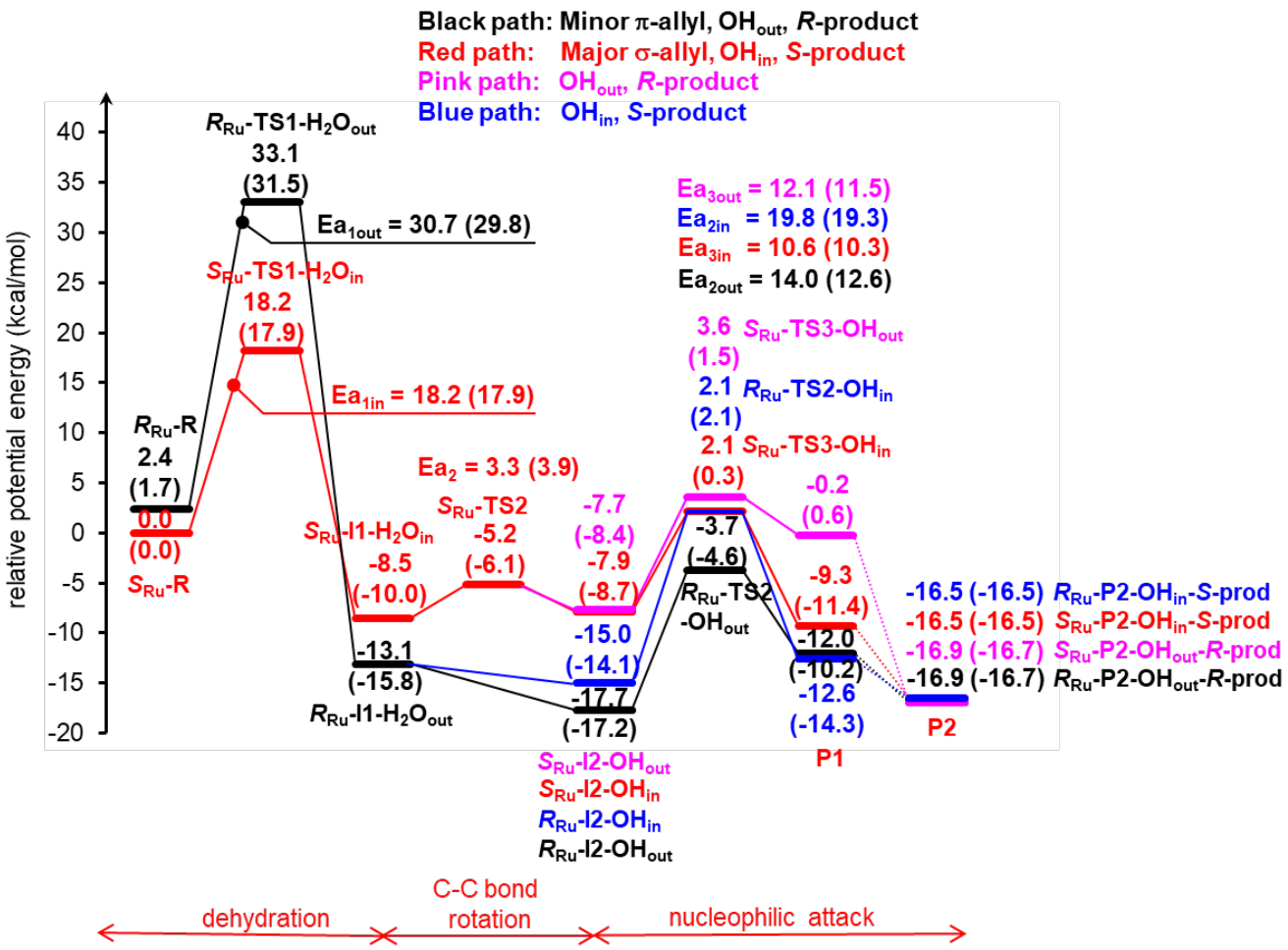

Figure 4. Potential energy profiles for (*R*)-Cl-Naph-PyCOOH–CpRu catalyzed intramolecular O-allylation via major σ-allyl mechanism (red), minor π-allyl mechanism (black) and possible routes OH_{out}, *R*-product (pink) with OH_{in}, *S*-product (blue). Gibbs free energies (298.15 K) are shown in parenthesis.

4.2.1 Major σ-Allyl Mechanisms (Pathways shown in red and pink)

As shown in Figure 5, the major σ-allyl mechanism (red) relies on both hydrogen bond (1.661 Å) and halogen bond (2.988 Å) to stabilize the catalyst-substrate R complex (S_{Ru}-R). This enables the H_2O_{in} pathway via TS1 (S_{Ru}-TS1-H_2O_{in}), with Ea_{1in} = 18.2 kcal mol^{-1} ($\Delta G^{‡}$ = 17.9 kcal mol^{-1}), to give the σ-allyl intermediate I1 (S_{Ru}-I1-H_2O_{in}). The calculated activation energy is in reasonable agreement with the experimentally determined activation energy (19.01 kcal mol^{-1} from the Eyring plot at 353 K[38] and 23.5 kcal mol^{-1} from the Freedman plot).[25] We distinguished between σ-allyl and π-allyl characters by considering 5 keys bond distances (C_1-C_2, C_2-C_3, Ru-C_1, Ru-C_2, and Ru-C_3). Thus, the distances C_1-C_2 = 1.417 Å, C_2-C_3 = 1.367 Å of allyl alcohol substrate and Ru-C_1 = 2.108 Å, Ru-C_2 = 2.217 Å, Ru-C_3 = 2.457 Å indicate that the σ-allyl character is prevalent in the I1 intermediate. The double attractive interactions through hydrogen and halogen bonds also aid in the formation of the σ-allyl complex. We note that alternative possibility of oxidative addition was ruled out due to unfavorable energetics as shown in Figure S4 in SI. Then, the σ-allyl intermediate I1 (ΔE = −8.5 kcal mol^{-1}, ΔG = −10.0 kcal mol^{-1}) changed its conformation to the σ-allyl intermediate I2 (ΔE = −7.9 kcal mol^{-1}, ΔG = −8.7 kcal mol^{-1}) via the C−C bond rotation (S_{Ru}-TS2) with a small barrier (Ea_2 = 3.3 kcal mol^{-1} ($\Delta G^{‡}$ = 3.9 kcal mol^{-1}). The nucleophilic OH_{in} pathway via TS3 (S_{Ru}-TS3-OH_{in}), with Ea_{3in} = 10.6 kcal mol^{-1} ($\Delta G^{‡}$ = 10.3 kcal mol^{-1}) is then used to generate the P1 major (*S*)-product complex (ΔE = −9.3 kcal mol^{-1}, ΔG = −11.4 kcal mol^{-1}). Finally, we identified the most stable P2 (S_{Ru}-P2-OH_{in}-*S*-prod) major (*S*)-product complex (ΔE = −16.5 kcal mol^{-1}, ΔG = −16.5 kcal mol^{-1}), where H_2O could stabilize both the catalyst and the product. This result indicated that the process is exothermic.

The pink path depicts another possible pathway (see the details of structures in Figure S2). The OH nucleophile can attack the C_3 of the allyl alcohol substrate from the outside (S_{Ru}-I2-OH_{out}) via TS3

(S_{Ru}-TS3-OH_{out}) with Ea_{3out} = 12.1 kcal mol^{-1} ($\Delta G^{\ddagger}$ = 11.5 kcal mol^{-1}) to generate the P1 minor (*R*)-product complex ($\Delta E = -0.2$ kcal mol^{-1}, ΔG = 0.6 kcal mol^{-1}). However, a proton from the OH group remain bonded in the P1 structure. A positional reorganization of H_2O would be required to return the proton back to the catalyst. Finally, the most stable P2 (S_{Ru}-P2-OH_{out}-*R*-prod) with (*R*)-product complex was identified, and the catalyst could be regenerated through an exothermic process with $\Delta E = -16.9$ kcal mol^{-1} ($\Delta G = -16.7$ kcal mol^{-1}). As a result, red pathway is the most favorable route for the dehydrative O−allylation reaction. According to the potential energy profile shown in Figure 4, the RDS for this reaction is dehydrative σ-allyl formation whereas the stereodetermining step in the $A_{S,in,in}$ catalytic cycle is the TS3 for nucleophilic attack.

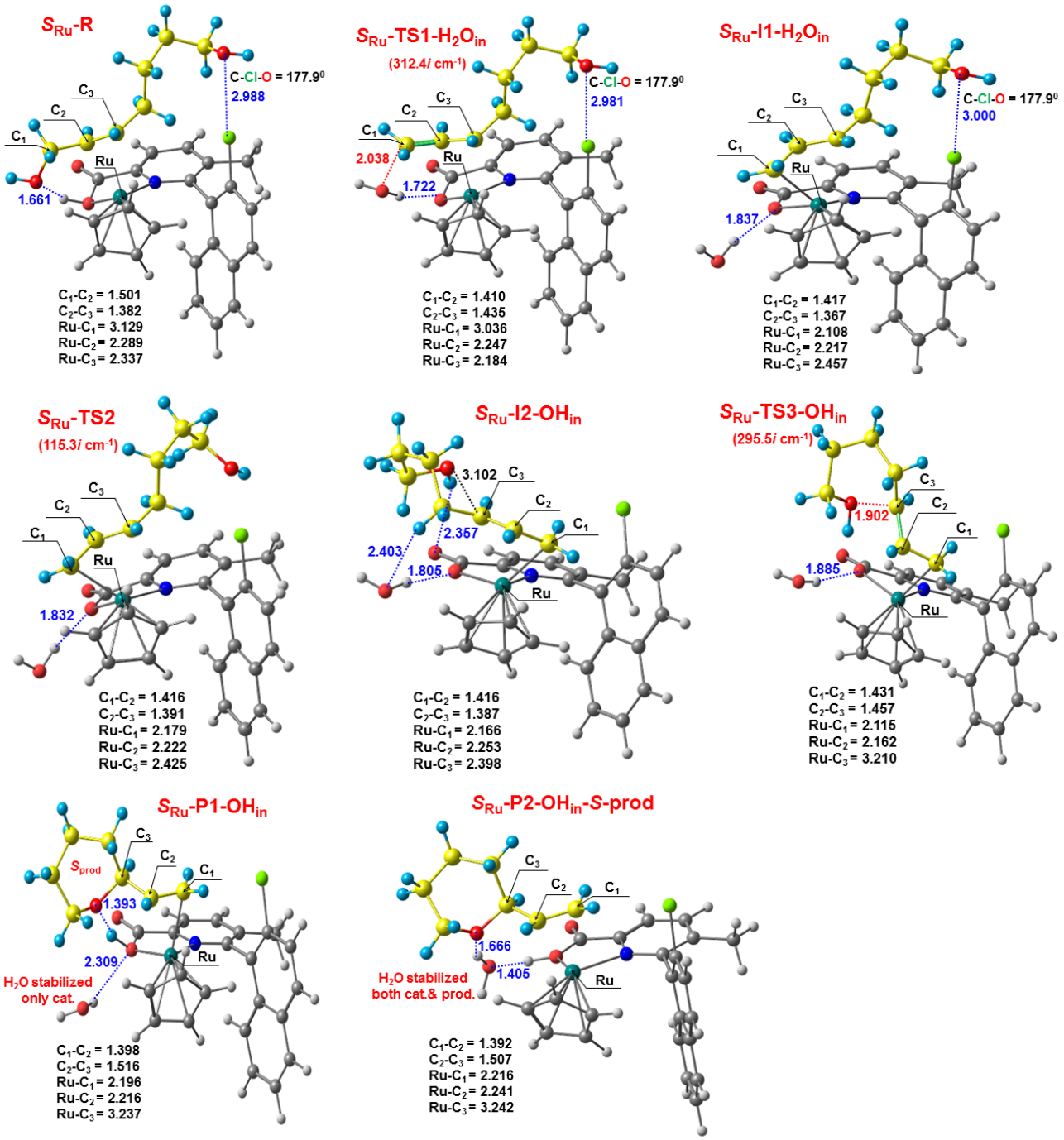

Figure 5. Optimized structures of intermediates and transition states for the CpRu−catalyzed asymmetric dehydrative O−allylation of the (*R*)−Cl−Naph−PyCOOH ligand via the major σ−allyl mechanism (red). Hydrogen bond and halogen bond distances are displayed in blue color. Bond distances are given in Å. The positions of C_1, C_2, C_3, Ru atoms are given in all structures.

4.2.2 Minor π−Allyl Mechanisms (Pathways shown in black and blue)

As for the minor π−allyl mechanism (black), the distances of C_1−C_2, C_2−C_3, Ru−C_1, Ru−C_2, and Ru−C_3 of all intermediates and transition states as presented in Figure 6. The reactant complex (R_{Ru}-R), which lacks both hydrogen and halogen bonds (Figure 6), is formed through the H_2O_{out} pathway via TS1 (R_{Ru}-TS1-H_2O_{out}), with Ea_{1out} = 30.7 kcal mol^{-1} $\Delta G^{\ddagger}$ = 29.8 kcal mol^{-1}), to give the stable π−allyl intermediate I1 (R_{Ru}-I1-H_2O_{out}; ΔE = −13.1 kcal mol^{-1}, ΔG = −15.8 kcal mol^{-1}). Unlike the red pathway, the C_1−C_2 and C_2−C_3 distances in the black pathway are 1.417 Å and 1.402 Å, respectively, and the Ru−C_1, Ru−C_2, and Ru−C_3 distances are 2.171 Å, 2.180 Å, and 2.328 Å, respectively. Those bond distances suggest that the π−allyl Ru intermediate takes place. Then, both the catalyst and substrate are stabilized by two hydrogen bonds with H_2O to generate the more stable π−allyl intermediate I2 (R_{Ru}-I2-H_2O_{out}; (ΔE = −17.7 kcal mol^{-1}, ΔG = −17.2 kcal mol^{-1}). Next, the OH_{out} pathway follows via TS2 (R_{Ru}-TS2-OH_{out}), with Ea_{2out} = 14.0 kcal mol^{-1} ($\Delta G^{\ddagger}$ = 12.6 kcal mol^{-1}), to generate the P1 minor (*R*)−product complex (ΔE = −12.0 kcal mol^{-1}, ΔG = −10.2 kcal mol^{-1}). In this structure, a proton from the OH group is still attached. A positional reorganization of H_2O would be necessary to return the proton back to the catalyst. Finally, we identified the most stable P2 minor (*R*)−product complex, and the catalyst could be regenerated through an exothermic process with ΔE = −16.9 kcal mol^{-1} (ΔG = −16.7 kcal mol^{-1}).

The blue path represents another possible pathway (see the details of structures in Figure S3). The OH nucleophile can attack the C_3 of the allyl alcohol substrate from inside (R_{Ru}-I2-OH_{in}) via TS2 (R_{Ru}-TS2-OH_{in}), with Ea_{2in} = 19.8 kcal mol^{-1} ($\Delta G^{\ddagger}$ = 19.3 kcal mol^{-1}), to generate the P1 major (*S*)-product complex (ΔE = −12.6 kcal mol^{-1}, ΔG = −14.3 kcal mol^{-1}). However, in P1 structure, the H_2O can only stabilize catalyst, requiring a positional reorganization of H_2O. Finally, we identified the most

stable P2 (R_{Ru}-P2-OH_{in}-*S*-prod) with (*S*)-product complex with $\Delta E = -16.9$ kcal mol^{-1} ($\Delta G = -16.7$ kcal mol^{-1}).

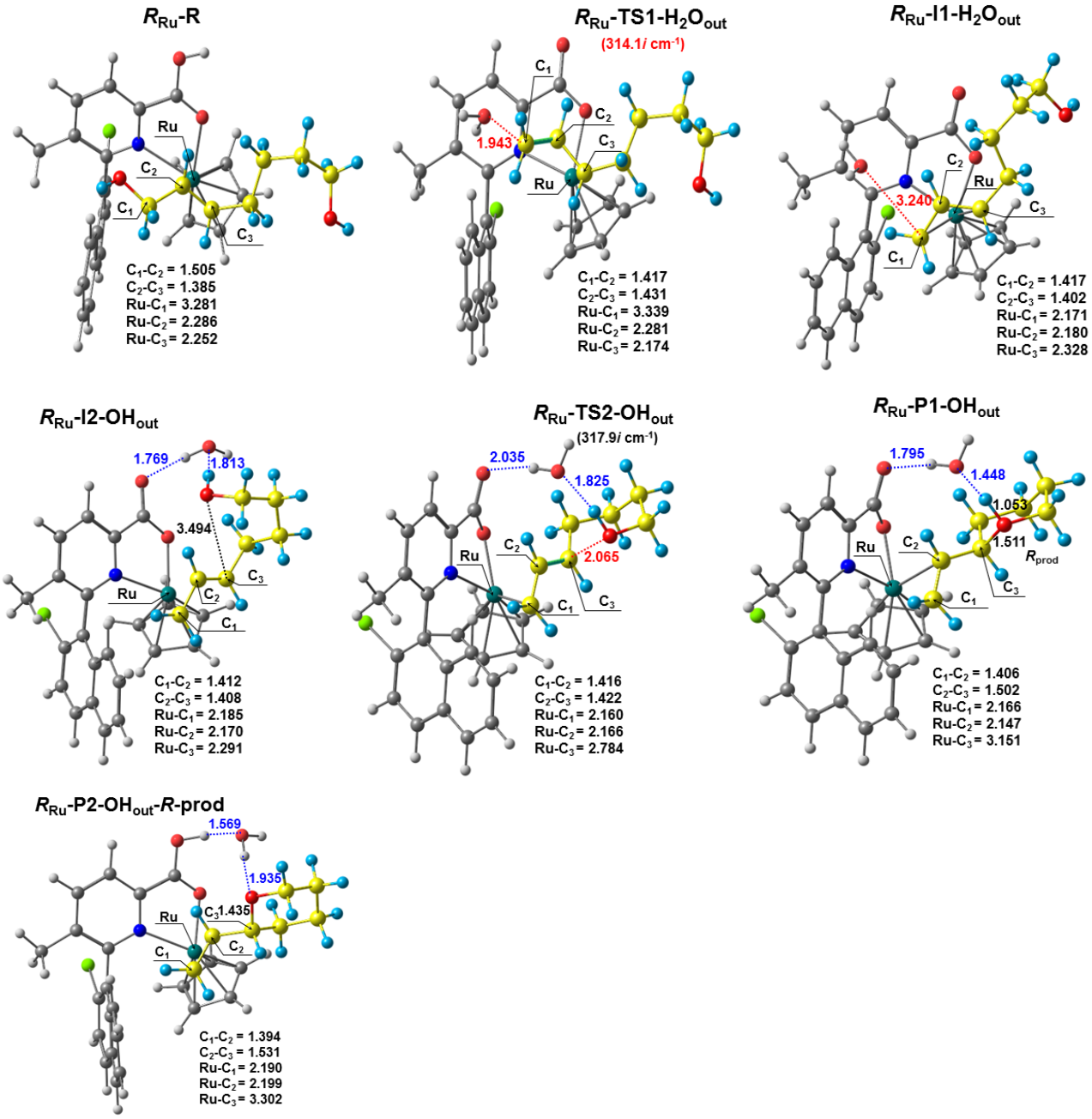

Figure 6. Optimized structures of intermediates and transition states for the CpRu−catalyzed asymmetric dehydrative O−allylation of the (*R*)−Cl−Naph−PyCOOH ligand via the minor π−allyl mechanism (black). Hydrogen bond and halogen bond distances are displayed in blue color. Bond distances are given in Å. The positions of C_1, C_2, C_3, Ru atoms are given in all structures.

In addition, the natural bond orbital (NBO) bond order analysis was performed for σ-Ru allyl complex using S_{Ru}-I1-H_2O_{in} (red path) and π-Ru allyl complex using R_{Ru}-I1-H_2O_{out} (black path) structures as given in Table S3 of the supporting information (SI). For the σ-Ru allyl intermediate (red path), the bond order for the C_1-C_2 and C_2-C_3 was calculated to be 0.97 and 1.65, respectively, indicating the property of single and double bonds for the C_1-C_2 and C_2-C_3 bond. For the π-Ru allyl intermediate (black path), the result for the C_1-C_2 and C_2-C_3 bond was both 0.97, indicating the characteristic of the π-allyl species.

In summary, the DFT calculations supported the mechanism of our earlier experimental study.[25] It was revealed that hydrogen and halogen bonds were crucial in facilitating the *R*,S_{Ru}−catalyzed reaction pathway via a σ−allyl intermediate to give the major (*S*)−product. The minor (*R*)−enantiomer is slowly generated either via a π−allyl intermediate (black pathway) or via the S_{Ru}-TS3-OH_{out} state (pink pathway). The results of these DFT calculations could explain the origin of the high enantioselectivity for (*R*)−Cl−Naph−PyCOOH−CpRu−catalyzed intramolecular O−allylation.

4.3 Halogen Bond Effect on the Reactivity

Besides hydrogen bonding,[32] halogen bonds[33−37] are classified into non−covalent interactions and have attracted attention because their bonding property are similar to those of hydrogen bonds. Based on our earlier experimental results,[25] the ligand structure/reactivity/selectivity relationship was investigated. The results showed that the replacement of the ligand's Cl atom with bromine or iodine atoms increased the initial rate as the strength of the halogen bond increased from Cl to Br to I atoms. The reactivity of the allylic alcohol substrate **2** improved in the order Cl (23%–30% conversion (convn)), Br (51%–58% convn), and I (34%–71% convn) in the X−Naph−PyCOOH ligands. Recently, we also explored the halogen effect on the reactivity with pyrroles substrate using the same catalysts.

The reactivity also increased from X = Cl (9% convn) to Br (65% convn), and I (>99% convn) in the same ligands.[39]

Figure 7 depicts optimized structures involved in RDS, S_{Ru}-*R*, S_{Ru}-TS1-H_2O_{in}, and S_{Ru}-I1-H_2O_{in} states, for X = Cl, Br, and I in the σ−allyl case. In the R state, the O−I bond was the shortest (2.638 Å), followed by the O−Br bond (2.828 Å), and then the O−Cl bond (2.998 Å). These bond lengths were nearly constant during the RDS. The strength of the σ−hole interaction can be explained by the second−order perturbation theory analysis in the NBO calculations. For the Cl, Br, and I chiral ligands, the orbital interaction between the lone pair of oxygen and σ*(C−X) of the σ−allyl intermediate I1 are 1.7 kcal mol^{-1}, 5.0 kcal mol^{-1}, 15.0 kcal mol^{-1}, respectively (see Table S1 in the SI).

The most plausible S_{Ru} pathway (red path) proceeds via H_2O liberation (H_2O_{in}), the RDS of this reaction. The Gibbs free energy barrier ($\Delta G^{‡}$) of RDS in the major σ−allyl mechanism at 353 K (80°C) was calculated and compared as shown in Table 1. The lowest activation energy was obtained for I−Naph−PyCOOH ligand (E_a^{RDS} = 15.3 kcal mol^{-1}, $\Delta G^{‡}$ = 14.4 kcal mol^{-1}), followed by the Br−Naph−PyCOOH ligand (E_a^{RDS} = 17.1 kcal mol^{-1}, $\Delta G^{‡}$ = 16.8 kcal mol^{-1}) and Cl−Naph−PyCOOH ligand (E_a^{RDS} = 18.2 kcal mol^{-1}, $\Delta G^{‡}$ = 18.1 kcal mol^{-1}); this is in line with the conversion in our previous experiment.[25]

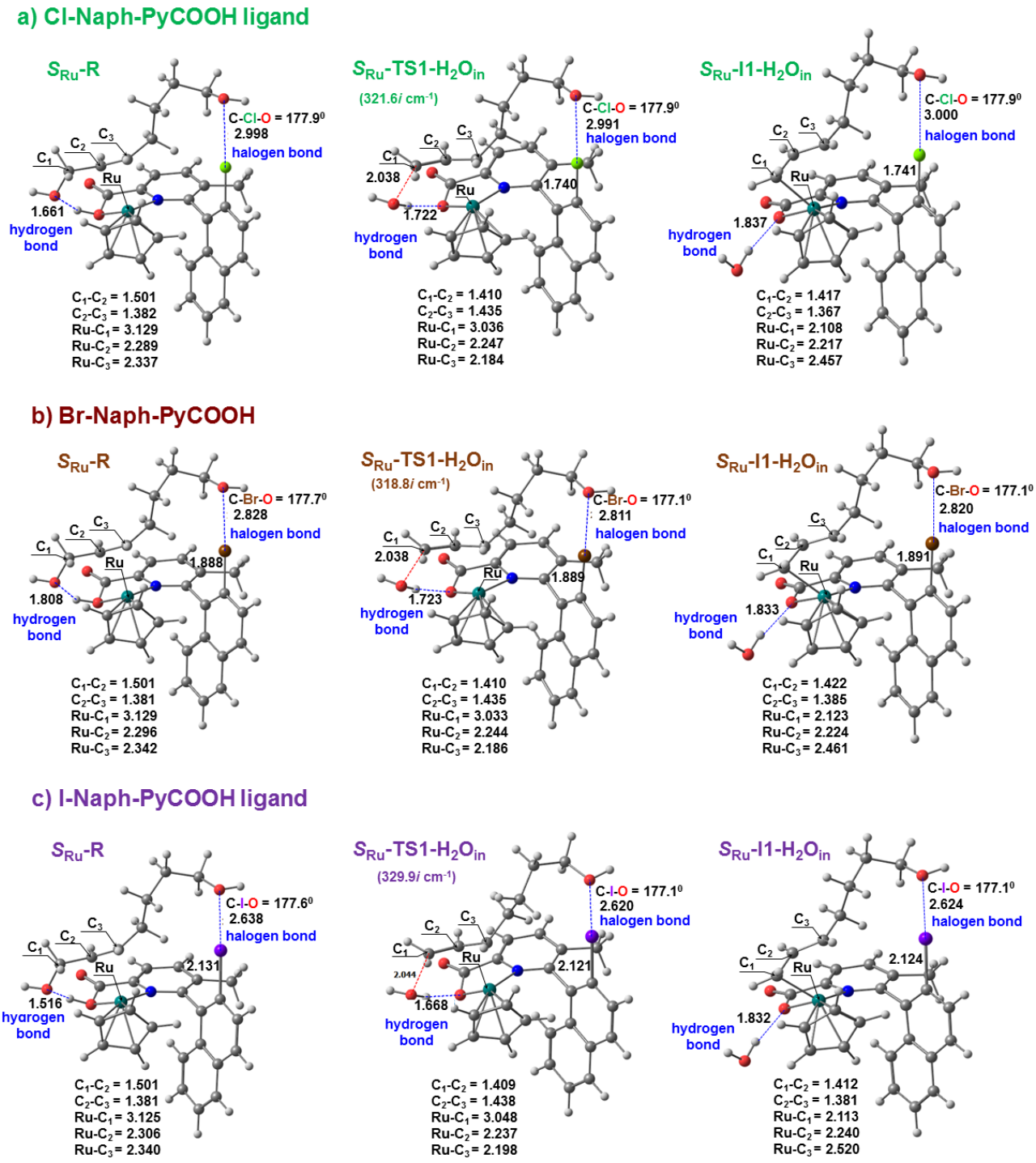

Figure 7. Optimized structures of reactant (S_{Ru}-*R*), transition state (S_{Ru}-TS1-H_2O_{in}), and the σ−allyl intermediate S_{Ru}-I1-H_2O_{in} of the RDS from the major σ−allyl mechanism (red pathway) using a) (*R*)−Cl−Naph−PyCOOH ligand, b) (*R*)−Br−Naph−PyCOOH ligand, and c) (*R*)−I−Naph−PyCOOH

ligand. Bond distances are given in Å. Hydrogen bond and halogen bond distances are displayed in blue color. The positions of C_1, C_2, C_3, Ru atoms are given in all structures.

Table 1. Comparison of the experimental results and values obtained from the DFT calculations of three chiral (*R*)−X−Naph−PyCOOH ligands (X = Cl, Br, I). Units for energies are in kcal/mol.

	Exptl[a]		DFT calculations results for RDS (TS1 H_2O_{in})[e]					
X ligand	$\Delta G^{‡}$	convn	E_a^{RDS}	$\Delta G^{‡}$	ΔE_r^{RDS}	ΔG_r	Halogen bond[f]	Hydrogen bond[g]
Cl	19.01[b],23.5[c]	23–30, 9[d]	18.2	18.1	−8.5	−10.3	2.998	1.661
Br		51–58, 65[d]	17.1	16.8	−10.7	−12.4	2.828	1.808
I		34–71, 99[d]	15.3	14.4	−13.2	−15.8	2.638	1.516

[a] "convn" denotes conversion in %.
[b] Experimental $\Delta G^{‡}$ at 353K obtained by the Eyring method.[38]
[c] Experimental E_a. See reference [25].
[d] For pyrrole N-tethered allylic alcohol.[39]
[e] "E_a^{RDS}" and "ΔE_r^{RDS}" denote activation energy and reaction energy, respectively, at potential energy level. "$\Delta G^{‡}$" and "ΔG_r" denote activation free energy and reaction free energy, respectively, calculated as relative Gibbs energy.
[f] "Halogen bond" is the O−X distance (Å) of the catalyst−substrate R complex (B_S−sa*Si*).
[g] "Hydrogen bond" is the H−O distance (Å) of the catalyst−substrate R complex (B_S−sa*Si*).

To clarify the origin of the observed halogen trend in activation energy, a structural decomposition analysis was conducted as shown in Figure 8. Starting with the original structure, the computational model was modified step−by−step to qualitatively evaluate the intramolecular interactions; (1) to evaluate the direct contribution of the halogen bond energy to the activation energy, the OH group at C_7 in the substrate was substituted by H atom, "w/o OH group (fixed)". This step is aimed at clarifying the contribution from halogen-substrate interaction via σ–hole. The "original" model's atomic coordinates are fixed. The interaction by the newly added H atom does not affect conclusion of the analysis as described in section S8 of supporting information. (2) All the atomic coordinates in (1)

were relaxed "w/o OH group (optimized)". (3) To turn off the halogen-substrate interaction, the halogen atom was substituted by a H atom, "w/o halogen (fixed)", and the structure was kept to the same as "original" one. Combining the result of step (1), this step can clarify the effect of the halogen-substrate interaction that does not involve σ–hole. Because the atomic coordinates are fixed, the direct contribution from the halogen-substrate interaction is distinguished from the contribution of the substrate strain. (4) In the final step, the halogenated naphthyl group was substituted by H atom, "w/o halogenated naphthyl group (fixed)". The role of the naphthyl-substrate interaction is clarified with this step. These structural changes were made to R and TS1, and the changes in activation energy were evaluated.

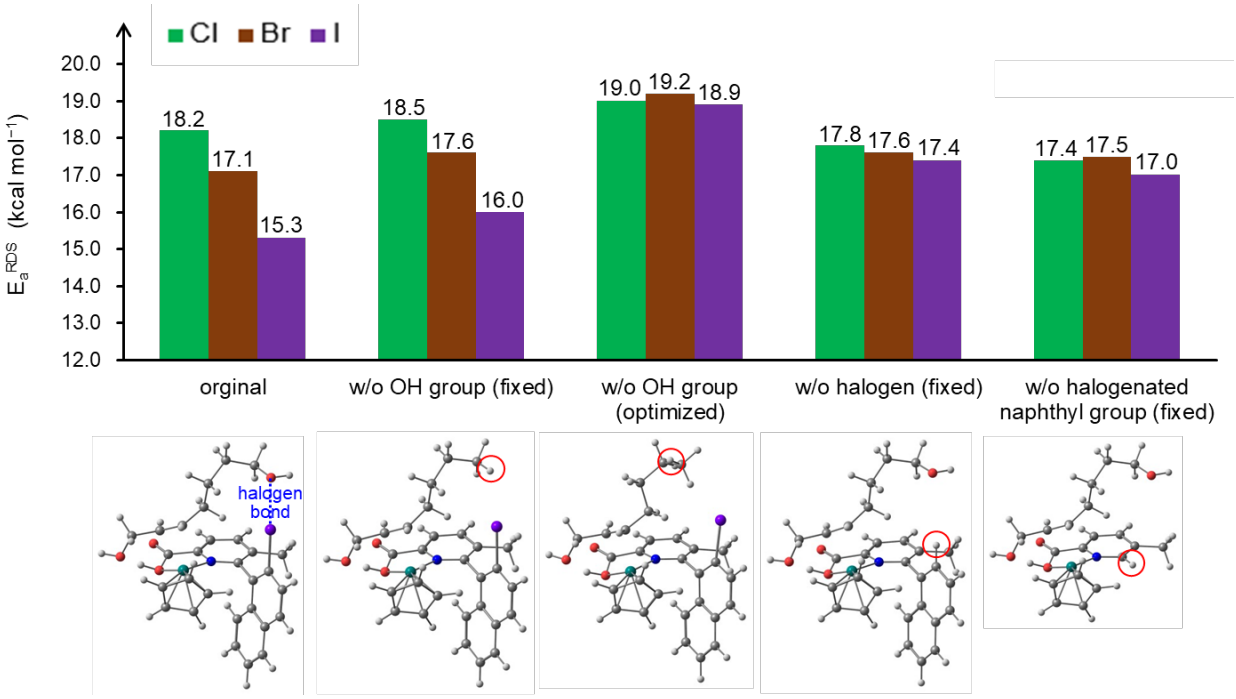

Figure 8. A structural decomposition analysis for the activation energy of RDS. The computational structures were modified step by step as shown in the structure drawings. The "original" denotes the optimized structures of the full model as shown in Figure 5. The "w/o OH group", "w/o halogen", and "w/o halogenated naphthyl group" denote that the OH group of the substrate, the halogen atom, and

the halogenated naphthyl group were replaced by a H atom, respectively. The position of the H atom was optimized. The "(fixed)" indicates that the structure was fixed to the original one, while the "(optimized)" denotes the structures were fully optimized.

With the result of the structural decomposition analysis, the origin of the halogen trend in the activation energy (E_a^{RDS}), Cl > Br > I, was interpreted. In the step (1), the halogen trend remains, showing that halogen bond energy has no direct energetic contribution to the halogen trend. The effect of the newly attached H atom was evaluated as shown in Table S6 of supporting information. The corrected "w/o OH group (fixed)" results for the Cl, Br, and I cases are 18.4 kcal/mol, 17.4 kcal/mol, and 16.3 kcal/mol, respectively, indicating the H substitution does not affect the present conclusion. Because the distance between H and halogen atoms during the reaction step are nearly constant, about 3.1 Å, 2.9 Å, and 2.8 Å for X = Cl, Br, and I, respectively, the interaction itself is small.

In the step (2) where the structure was optimized, the trend disappears. The E_a^{RDS} for the I (iodide) case showed the largest increase by 3.0 kcal/mol, followed by the Br case by 1.7 kcal/mol. In Table S4 of supporting information, the structural relaxation energy due to the optimization was compared between the reactant and transition states. The result shows that the reactant state is more intensely relaxed than the transition state, and the magnitude of the relaxation is greater in the order I > Br > Cl. As a result, the activation energy of the I case increased most significantly after the optimization, that of the Br case follows, and that of the Cl case was the least susceptible to optimization. Table S4 also shows the halogen bond distances in the reactant and transition states. Only minor changes (−0.007 Å in Cl, −0.017 Å in Br, −0.018 Å in I) were observed in the halogen bond length. These results indicate that the halogen bond keeps the coordination structure of the substrate against the repulsive interaction between the halogen atom and the substrate.

In the third step, the halogen atom was deleted, “w/o halogen (fixed)”. This step switches off all the interactions between the halogen atom and substrate. This step can also clarify whether the origin of the halogen trend is caused by the structural strain energy of the substrate or by the interaction energy between the halogen atom and the substrate. As a result, the halogen trend disappeared almost completely even though the structure was fixed. Together with the result of the “w/o OH group (fixed)” model, the origin of the halogen trend is in the halogen-substrate interactions that do not involve σ–hole. To be sure, we also replaced the naphthyl group entirely, “w/o halogenated naphthyl group (fixed)”. The result was the same as that obtained with the “w/o halogen (fixed)” model, showing that the essential part of the origin was already removed at the “w/o halogen (fixed)” level.

The result would provide a following qualitative summary of the origin of the halogen trend emerges: the halogen bond energy does not directly contribute to the magnitude of the activation energy. However, the halogen bond, particularly for Br and I, is strong enough to maintain the substrate’s conformation in the presence of repulsive interactions between the halogen atom and the substrate. As shown in Table S1, the result of the NBO second-order perturbation theory analysis shows that these halogen bond interaction energies were 15.0 kcal/mol for I, and 5.0 kcal/mol for Br cases, indicating these attractive interactions would be strong enough to support the structure against the repulsive part of the halogen-substrate interaction. This repulsive interaction contributes directly to the halogen trend in the barrier height.

5 Conclusion

As the ruthenium−catalyzed asymmetric dehydrative cyclization of alcohol to cyclic ether has gained considerable attention, understanding its catalytic mechanism is vital. In the present study, we employed the DFT calculations to clarify the mechanism of the

(*R*)−Cl−Naph−PyCOOH−CpRu−catalyzed intramolecular O−allylation reaction. The calculation results indicated that the RDS is the dehydrative σ-allyl formation step, with E_a^{RDS} = 18.2 kcal mol^{-1} and $\Delta G^{\ddagger}$ = 18.1 kcal mol^{-1} at 80°C; this is in good agreement with the result of experimental kinetics analysis (E_a=23.5 kcal mol^{-1} and $\Delta G^{\ddagger}$=19.01 kcal mol^{-1} at 80°C). The origin of the enantioselectivity was elucidated using the catalyst/substrate complex (S_{Ru} and R_{Ru}). It is concluded that the hydrogen and halogen bonds play a crucial role in facilitating the major *R*,S_{Ru}−catalyzed reaction pathway via a σ−allyl Ru intermediate to give the major *S*−product. In particular, the COOH group in the ligands participated in both dehydration and O−allylation steps which not only reduced activation energy but also controlled the sterically favorable route to determine enantioselectivity. The minor *R*-product is formed via a conventional π-allyl Ru intermediate and via a minor cyclization pathway. Furthermore, the DFT calculations revealed that the order of reactivity of the (*R*)−X−Naph−PyCOOH ligands at 353K ($\Delta G^{\ddagger}$ of I (14.4 kcal mol^{-1}) < Br (16.8 kcal mol^{-1}) < Cl (18.1 kcal mol^{-1}) depends on the halogen bond effect which was clarified by a structural decomposition analysis. This DFT calculation results are consistent with our previous experimental studies.[25]

ASSOCIATED CONTENT

Supporting Information.

Results of second order perturbation theory analysis for the σ-hole interaction, determination of $\Delta G^{\ddagger}$ by Eyring plot, NBO bond order analysis, structural optimizations for the pink and blue pathways, potential energy curve for oxidative addition to the C-O bond, structural decomposition analysis, and the effect of basis sets extension in the single point calculations. Atomic coordinates for the

optimized structures. The supporting information is available free of charge on the ACS Publications website at DOI: XXXXXX/XXXXXXX.

AUTHOR INFORMATION

Corresponding Author

*E−mail for J.H.: hasegawa@cat.hokudai.ac.jp

*E−mail for M.K.: kitamura@os.rcms.nagoya−u.ac.jp

Notes

The authors declare no competing financial interest.

Acknowledgement

This work was supported by JSPS KAKENHI (JP15H05805, JP16H01014, JP18H04250, JP20H02685) and in part by the Cooperative Research Program of Institute for Catalysis, Hokkaido University. M.R. and J.H. appreciate financial support from the Photo-excitonix Project in Hokkaido University and the Integrated Research Consortium on Chemical Sciences (IRCCS). A part of the computational work was performed at RCCS in Okazaki, Japan (Project: 22-IMS-C002).

References

1. Trost, B. M.; Crawley, M. L., Asymmetric Transition−Metal−Catalyzed Allylic Alkylations: Applications in Total Synthesis. *Chem. Rev.* **2003,** *103* (8), 2921−2944.

2. Consiglio, G.; Indolese, A., Enantioselective Cross−Coupling of Vinyl−, Aryl− and Allyl−Electrophiles Catalyzed by Nickel Complexes Containing (R, R)−1,2−cyclopentanediylbis(diphenylphosphine) and Related Ligands. *J. Organomet. Chem.* **1991,** *417* (1−2), C36−C40.

3. Trost, B. M.; Hachiya, I., Asymmetric Molybdenum−Catalyzed Alkylations. *J. Am. Chem. Soc.* **1998,** *120* (5), 1104−1105.

4. Selvakumar, K., Valentini, M., Pregosin, P. S.; Albinati, A., Chiral Phosphito−Thioether Complexes of Palladium(0). Comments on the Pd, Rh, and Ir Regio− and−Enantioselective Allylic Alkylations of PhCHCHCH(OAc)R, R = H, Me, Et. *Organometallics* **1999,** *18* (22), 4591−4597.

5. Janssen, J. P.; Helmchen, G., First Enantioselective Alkylations of Monosubstituted Allylic Acetates Catalyzed by Chiral Iridium Complexes. *Tetrahedron Lett.* **1997,** *38* (46), 8025−8026.

6. Brown, J. M.; Maclntyre, J. E., Allylic Alkylation Catalysed by Platinum Complexes; Structure and Reactivity of Intermediates, and the Overall Stereoselectivity. *J. Chem. Soc. Perkin Trans. 2* **1985,** *7* (7), 961−970.

7. Lloyd−Jones, G. C.; Pfaltz, A., Chiral Phosphanodihydrooxazoles in Asymmetric Catalysis: Tungsten−Catalyzed Allylic Substitution. *Angew. Chem. Int. Ed. Engl.* **1995,** *34* (4), 462−464.

8. Trost, B. M.; Van Vranken, D. L., Asymmetric Ligands for Transition−Metal−Catalyzed Reactions: 2−Diphenylphosphinobenzoyl Derivatives of C2−Symmetric Diols and Diamines. *Angew. Chem. Int. Ed. Engl.* **1992,** *31* (2), 228−230.

9. Trost, B. M., Van Vranken, D. L.; Bingel, C., A Modular Approach for Ligand Design for Asymmetric Allylic Alkylations via Enantioselective Palladium−Catalyzed Ionizations. *J. Am. Chem. Soc.* **1992,** *114* (24), 9327−9343.

10. Trost, B. M., Metal Catalyzed Allylic Alkylation: Its Development in the Trost Laboratories. *Tetrahedron* **2015,** *71* (35), 5708−5733.

11. Tsuji, J., Kiji, J., Imamura, S.; Morikawa, M., Organic Syntheses by Means of Noble Metal Compounds. VIII.1 Catalytic Carbonylation of Allylic Compounds with Palladium Chloride. *J. Am. Chem. Soc.* **1964,** *86* (20), 4350−4353.

12. Sundararaju, B., Achard, M.; Bruneau, C., Transition Metal Catalyzed Nucleophilic Allylic Substitution: Activation of Allylic Alcohols via π−Allylic Species. *Chem. Soc. Rev.* **2012,** *41* (12), 4467−4483.

13. Yamashita, Y., Gopalarathnam, A.; Hartwig, J. F., Iridium−Catalyzed, Asymmetric Amination of Allylic Alcohols Activated by Lewis Acids. *J. Am. Chem. Soc.* **2007,** *129* (24), 7508−7509.

14. Roggen, M.; Carreira, E. M., Stereospecific Substitution of Allylic Alcohols to Give Optically Active Primary Allylic Amines: Unique Reactivity of a (P,Alkene)Ir Complex Modulated by Iodide. *J. Am. Chem. Soc.* **2010,** *132* (34), 11917−11919.

15. Bandini, M.; Eichholzer, A., Enantioselective Gold−Catalyzed Allylic Alkylation of Indoles with Alcohols: An Efficient Route to Functionalized Tetrahydrocarbazoles. *Angew. Chem. Int. Ed. Engl.* **2009,** *48* (50), 9533−9537.

16. Yamamoto, H., Ho, E., Namba, K., Imagawa, H.; Nishizawa, M., Hg(OTf)2–BINAPHANE−Catalyzed Enantioselective Anilino Sulfonamide Allyl Alcohol Cyclization. *Chem. Eur. J.* **2010,** *16* (37), 11271−11274.

17. Jiang, G.; List, B., Direct Asymmetric α−Allylation of Aldehydes with Simple Allylic Alcohols Enabled by the Concerted Action of Three Different Catalysts. *Angew. Chem. Int. Ed. Engl.* **2011,** *50* (40), 9471−9474.

18. Shin, I., Wang, G.; Krische, M. J., Catalyst−Directed Diastereo− and Site−Selectivity in Successive Nucleophilic and Electrophilic Allylations of Chiral 1,3−Diols: Protecting−Group−Free Synthesis of Substituted Pyrans. *Chemistry* **2014,** *20* (41), 13382−13389.

19. Biannic, B.; Aponick, A., Gold−Catalyzed Dehydrative Transformations of Unsaturated Alcohols. *Eur. J. Org. Chem.* **2011**, *2011* (33), 6605−6617.

20. Piechaczyk, O., Thoumazet, C., Jean, Y.; le Floch, P., DFT Study on the Palladium−Catalyzed Allylation of Primary Amines by Allylic Alcohol. *J. Am. Chem. Soc.* **2006,** *128* (44), 14306−14317.

21. Huo, X., Yang, G., Liu, D., Liu, Y., Gridnev, I. D.; Zhang, W., Palladium−Catalyzed Allylic Alkylation of Simple Ketones with Allylic Alcohols and Its Mechanistic Study. *Angew. Chem. Int. Ed. Engl.* **2014,** *53* (26), 6776−6780.

22. McPherson, K. E., Croatt, M. P., Morehead, A. T.; Sargent, A. L., DFT Mechanistic Investigation of an Enantioselective Tsuji–Trost Allylation Reaction. *Organometallics* **2018,** *37* (21), 3791−3802.

23. Wang, D.; Li, C.−J., Mono−Alkylation of Diols Through Ruthenium−Catalyzed Reaction with Homoallyl Alcohols. *Synth. Commun.* **1998,** *28* (3), 507−515.

24. Hermatschweiler, R., Fernández, I., Pregosin, P. S., Watson, E. J., Albinati, A., Rizzato, S., Veiros, L. F.; Calhorda, M. J., X−Ray, 13C NMR, and DFT Studies on a Ruthenium(IV) Allyl Complex. Explanation for the Observed Control of Regioselectivity in Allylic Alkylation Chemistry. *Organometallics* **2005,** *24* (8), 1809−1812.

25. Suzuki, Y., Iwase, S., Ratanasak, M., Hasegawa, J.−y., Tanaka, S.; Kitamura, M., Mechanism of the Asymmetric Dehydrative Allylative Cyclization of Alcohols to Cyclic Ethers Catalyzed by a CpRu Complex of the Chiral Picolinic Acid−Type Ligand, Cl−Naph−PyCOOH: Is a π−Allyl Intermediate Present? *Bull. Chem. Soc. Jpn.* **2021,** *94* (2), 440−450.

26. Saburi, H., Tanaka, S.; Kitamura, M., Catalytic Dehydrative Allylation of Alcohols. *Angew. Chem. Int. Ed. Engl.* **2005,** *44* (11), 1730−1732.

27. Tanaka, S., Suzuki, Y., Kimura, T.; Kitamura, M., A Chiral Picolinic Acid Ligand, Cl−Naph−PyCOOH, for CpRu−Catalyzed Dehydrative Allylation: Design, Synthesis, and Properties. *Bull. Chem. Soc. Jpn.* **2019,** *92* (10), 1707−1720.

28. Frisch, M. J., Trucks, G. W., Schlegel, H. B., Scuseria, G. E., Robb, M. A., Cheeseman, J. R., Scalmani, G., Barone, V., Mennucci, B., Petersson, G. A., Nakatsuji, H., Caricato, M., Li, X., Hratchian, H. P., Izmaylov, A. F., Bloino, J., Zheng, G., Sonnenberg, J. L., Hada, M., Ehara, M., Toyota, K., Fukuda, R., Hasegawa, J., Ishida, M., Nakajima, T., Honda, Y., Kitao, O., Nakai, H., Vreven, T., Montgomery, J. A., Jr., Peralta, J. E., Ogliaro, F., Bearpark, M., Heyd, J. J., Brothers, E., Kudin, K. N., Staroverov, V. N., Kobayashi, R., Normand, J., Raghavachari, K., Rendell, A., Burant, J. C., Iyengar, S. S., Tomasi, J., Cossi, M., Rega, N., Millam, J. M., Klene, M., Knox, J. E., Cross, J. B., Bakken, V., Adamo, C., Jaramillo, J., Gomperts, R., Stratmann, R. E., Yazyev, O., Austin, A. J., Cammi, R., Pomelli, C., Ochterski, J. W., Martin, R. L., Morokuma, K., Zakrzewski, V. G., Voth, G. A., Salvador, P., Dannenberg, J. J., Dapprich, S., Daniels, A. D., Farkas, Ö., Foresman, J. B., Ortiz, J. V., Cioslowski, J.; Fox, D. J., Gaussian 09, Revision E.01. *Gaussian, Inc.,* Wallingford *CT* **2009**.

29. Chai, J. D.; Head−Gordon, M., Long−Range Corrected Hybrid Density Functionals with Damped Atom–Atom Dispersion Corrections. *Phys. Chem. Chem. Phys.* **2008,** *10* (44), 6615−6620.

30. Martin, J. M. L.; Sundermann, A., Correlation Consistent Valence Basis Sets for Use with the Stuttgart–Dresden–Bonn Relativistic Effective Core Potentials: The Atoms Ga–Kr and In–Xe. *J. Chem. Phys.* **2001,** *114* (8), 3408−3420.

31. Zhurko, G. A.; Zhurko, D. A. Chemcraft, Chemcraft, version 1.8. https://www.chemcraftprog.com.

32. Alkorta, I., Rozas, I.; Elguero, J., Non−Conventional Hydrogen Bonds. *Chem. Soc. Rev.* **1998,** *27* (2), 163−170.

33. Wilcken, R., Zimmermann, M. O., Lange, A., Joerger, A. C.; Boeckler, F. M., Principles and Applications of Halogen Bonding in Medicinal Chemistry and Chemical Biology. *J. Med. Chem.* **2013,** *56* (4), 1363−1388.

34. Cavallo, G., Metrangolo, P., Milani, R., Pilati, T., Priimagi, A., Resnati, G.; Terraneo, G., The Halogen Bond. *Chem. Rev.* **2016,** *116* (4), 2478−2601.

35. Beale, T. M., Chudzinski, M. G., Sarwar, M. G.; Taylor, M. S., Halogen Bonding in Solution: Thermodynamics and Applications. *Chem. Soc. Rev.* **2013,** *42* (4), 1667−1680.

36. Desiraju, G. R., Ho, P. S., Kloo, L., Legon, A. C., Marquardt, R., Metrangolo, P., Politzer, P., Resnati, G.; Rissanen, K., Definition of the Halogen Bond (IUPAC Recommendations 2013). *Pure Appl. Chem.* **2013,** *85* (8), 1711−1713.

37. Politzer, P., Lane, P., Concha, M. C., Ma, Y.; Murray, J. S., An Overview of Halogen Bonding. *J. Mol. Model.* **2007,** *13* (2), 305−311.

38. Calculated activation free energy by the Eyring method. Activation energy ($\Delta G^{\ddagger}$)=19.01 kcal/mol at 80°C (353K) for (*R*)−Cl−Naph−PyCOOH ligand. For the details, see Figure S1 in the SI.

39. Iwase, S.; Suzuki, Y.; Tanaka, S.; Kitamura, M., CpRu/Brønsted Acid-Catalyzed Enantioselective Dehydrative Cyclization of Pyrroles N-Tethered with Allylic Alcohols. *Org. Lett.* **2020,** *22* (5), 1929-1933.

Table of contents graphics